Comput Mech
DOI 10.1007/s00466-013-0958-0

ORIGINAL PAPER

Coupling of discrete random walks and continuous modeling for three-dimensional tumor-induced angiogenesis

Guillermo Vilanova · Ignasi Colominas · Hector Gomez

Received: 30 June 2013 / Accepted: 29 November 2013

Abstract The growth of new vascular networks from pre-existing capillaries (angiogenesis) plays a pivotal role in tumor development. Mathematical modeling of tumor-induced angiogenesis may help understand the underlying biology of the process and provide new hypotheses for experimentation. Here, we couple an existing deterministic continuum theory with a discrete random walk, proposing a new model that accounts for chemotactic and haptotactic cellular migration. We propose an efficient numerical method to approximate the solution of the model. The accuracy, stability and effectiveness of our algorithms permitted us to perform large-scale three-dimensional simulations which, in contrast to two-dimensional calculations, show a topological complexity similar to that found in experiments. Finally, we use our model and simulations to investigate the role of haptotaxis and chemotaxis in the mobility of tip endothelial cells and its influence in the final vascular patterns.

Keywords Tumor angiogenesis · Isogeometric analysis · Numerical simulations · Random walk · Capillary growth

1 Introduction

Tumor growth may be understood as a multistage process. The cells forming the tumor, descendants of a single abnormal cell [74], acquire through mutations several malignant characteristics [39,40] that determine the stage wherein the tumor is. For many tumors, the first of these stages is avascular growth. At this stage, the tumor relies on diffusion mechanisms to get nutrients and to remove the waste products of the cell activity through nearby blood vessels and the lymphatic system. However, as the tumor grows, diffusion mechanisms become insufficient to maintain the high proliferation rate of tumor cells and those located far from the vessels enter non-proliferative hypoxic states or die from anoxia, starvation, or metabolic poisoning. Diffusion-limited growth imposes a threshold in the maximum diameter of an avascular tumor (usually between 1 and 2 mm [26]), for which the proliferative rate is balanced with the apoptotic rate [67]. The tumor may be years or decades immersed in the avascular stage [27] without causing any harm to the host tissue.

Eventually, a tumor cell may find a way to access nutrients and to eliminate wastes. One of these ways (first hypothesized by Folkman [26]) is to create its own blood supply through a process called angiogenesis: the creation of new capillaries from pre-existing ones. Endothelial cells, the cells that line blood vessels, are usually in a quiescent state tightly controlled by the balance of pro- and anti-angiogenic factors. This balance is only disrupted during the normal adult life in certain situations and for short periods of time, such as in wound healing or in the female reproductive cycle. Nevertheless, the genomic instability of tumor cells may lead to daughter cells that have gained the ability to control the balance of angiogenic factors, for example under hypoxic conditions. As a consequence, the tumor may overcome the size-limited avascular growth and enter the so-called vascular stage. This step, usually called the angiogenesis switch [12,27], is often related to a malignant state of the tumor, as cell proliferation is no longer limited and cells may enter the bloodstream and migrate to any part of the body, attaining the tumor the metastatic stage.

Electronic supplementary material The online version of this article (doi:10.1007/s00466-013-0958-0) contains supplementary material, which is available to authorized users.

G. Vilanova (✉) · I. Colominas · H. Gomez
Department of Applied Mathematics, University of A Coruña, Campus de Elviña, 15071 A Coruña, Spain
e-mail: gvilanovac@udc.es

Cancer cells use a number of strategies to unbalance the angiogenic factor equilibrium. Some of them can be quite sophisticated and cancer cells may even induce normal cells in their micro-environment to disrupt the angiogenic factor equilibrium on behalf of them [46]. A general assumption in mathematical modeling is that the process is governed by just one pro-angiogenic factor that diffuses from hypoxic cancer cells (see, for example, [54,56]). Regardless of the mechanism that cancer cells use to initiate angiogenesis, the first step of the cascade consists of endothelial cells receiving signals that spur them to switch their usual quiescent phenotype to a migratory one. These cells are commonly called tip endothelial cells and are responsible for leading the growth of new capillary sprouts towards the cells that demand an extra supply of blood components, and in the case of tumors, towards hypoxic cells. However, not all endothelial cells that receive the signal become migratory. The first-stimulated cells release a molecule, called delta-like ligand 4 (dll-4), that binds to the Notch receptors of the neighboring endothelial cells, impeding them to become tip endothelial cells [41]. Instead, these cells acquire a proliferative phenotype and form the stalk of the new capillary, being referred to as stalk cells for this reason.

The migration of the endothelial cells is thought to be driven by three coordinated mechanisms, namely, chemotaxis, haptotaxis and mechanotaxis [48]. Chemotaxis is defined as the movement following a gradient of concentration of a certain soluble chemical, in this case the soluble fraction of angiogenic factor. Haptotaxis is the motion driven by gradients of non-soluble chemoattractants bounded to the substrate of the extracellular matrix (in angiogenesis the fraction of angiogenic factor bounded to the extracellular matrix) or driven by gradients of focal adhesion sites. Both the non-soluble chemoattractants and the focal adhesion sites depend on the spatial distribution of the fibers of the extracellular matrix. As the characteristic length scale of the fiber distribution is significantly smaller than that of the global motion of the tip endothelial cells, haptotaxis may be understood as variations in the direction of cells movement. The last of these mechanisms, mechanotaxis, is the movement stimulated by mechanical forces. In order to capture all cues, tip endothelial cells develop multiple protrusions called filopodia [31].

In tumor angiogenesis, the growth of a capillary is driven by migration of tip endothelial cells and proliferation of stalk cells. The process finishes when tip cells find another endothelial cell in their way or the stimuli end. In the first situation, the tip endothelial cell connects with another capillary, fusing their lumina and forming loops, through a process called anastomosis [3]. This process is vital, for it allows the blood to circulate through the vessels. It is known that mechanotaxis plays a pivotal role in anastomosis [68], because it is one of the key mechanisms whereby tip endothelial cells detect each other. In the second situation, when the stimuli end, the capillary regresses under pathological conditions, such as in tumor-induced angiogenesis. The reason is that, unlike in physiological angiogenesis, the new capillaries induced by tumors are immature and stimuli dependent. Other features that characterize tumor capillaries are tortuosity, leakiness, high interstitial pressure, and poor blood flow, among others [25]. The delivery of drugs through the vascular system using nanoscale particles [22,28,50] is affected by these characteristics. In summary, vascular networks induced by tumors are defective and they create three-dimensional characteristic patterns.

Mathematical modeling of tumor angiogenesis may be divided into three categories: Continuous models at the cell-density level or macro-scale, discrete models at the cellular and sub-cellular level, and hybrid models that incorporate various scales. For a detailed review of the literature on this topic the reader is referred to [64]. Continuous models are usually systems of partial differential equations derived from physical and biological principles. They do not consider the cellular scale, so they usually do not capture the complex patterns of the vasculature. Examples of this type of models may be found in the references [5,51,52,59]. In contrast, discrete models study the behavior of each cell separately. This feature is specially relevant for the study of the movement of the tip endothelial cells [1,2,7,14,66]. A common approach is to model the migration of the tip cells as a random walk [11,13,29,71]. For example, based on the work of Hill and Häder for the trajectories of micro-organisms [42], Plank and Sleeman [62] modeled the migration of tip endothelial cells as a circular biased random walk [17]. However, their model and most discrete models do not explicitly include stalk cells and just assume they are in the migration path behind tip cells [29,61,62,70]. Another drawback of these models is their computational cost. Finally, hybrid models, such as [55,57,58,65] benefit from the computational simplicity of the continuous models, while still consider the cellular level. For example, Travasso et al. [23,72] proposed a hybrid model that accounts for the chemotactic migration of tip endothelial cells modeled as discrete agents and the proliferation of stalk cells governed by a high-order partial differential equation of the phase-field type.

Here, following the philosophy proposed in [4,14,15], we couple the hybrid deterministic model proposed by Travasso et al. [72] with a random walk model biased in the direction of chemotactic migration [69]. We believe that the stochastic component may represent a simple mathematical conceptualization of haptotaxis, a biological phenomenon whose underlying physics takes place at a significantly smaller spatial scale. We also propose an efficient computational method to approximate the solution to our model. The effectiveness of our method permitted us to perform large-scale simulations that show three-dimensional angiogenesis at a significant level of detail.

Journal: 466 MS: 0958 TYPESET DISK LE CP Disp.:2013/12/13 Pages: 16 Layout: Large

The rest of the paper is organized as follows: In Sect. 2, we derive the extended mathematical model of tumor induced angiogenesis that includes chemotaxis and haptotaxis. We explain separately the continuous partial differential equations of the macro-scale and the discrete agents at cellular level, and then explain the equations that couple both scales. We pay special attention to the movement of the tip endothelial cells governed by the biased circular random walk. In Sect. 3, we propose a numerical method to solve the mathematical model. We start by detailing the stochastic motion of tip endothelial cells, continue with the coupling methodology and finalize with the discretization of the partial differential equations. The numerical method allows us to perform two- and three-dimensional simulations of the mathematical model, as shown in Sect. 4. There, we perform a parametric study of the model through two-dimensional simulations. Then, supported by four simulations, we discuss the behavior of the model in three-dimensional settings and qualitatively characterize the vascular networks. At the end of the section we compare the mathematical models with and without haptotaxis. Finally, the conclusions and future work are presented in Sect. 5.

2 The mathematical model

This section presents the multi-scale, hybrid model proposed by Travasso et al. [72], and shows how we extended the model to account for haptotaxis, a relevant biological phenomenon that was not considered in the original model. Travasso et al. derived their model assuming that the hypoxic regions of the tissue release Tumor Angiogenic Factor (TAF) that is consumed by the endothelial cells. The model naturally describes the initiation of angiogenesis, which is controlled by discrete rules that evaluate the angiogenic factor and its gradient, additionally enforcing the Delta-Notch effect. Endothelial cells may exhibit a proliferative (stalk cells) or a migratory (tip cells) phenotype in the model, being the phenotype switch controlled by discrete rules. Hence, the growth of new capillaries is achieved by way of proliferation of stalk cells and migration of tip endothelial cells.

Here, we extend the model to account for haptotaxis during the migration of the tip endothelial cells. The original model treats this type of cells as discrete agents and assumes their movement to be deterministic and driven by chemotaxis. Thus, the velocity of tip endothelial cells is proportional to the gradient of the tumor angiogenic factor. We introduce a new definition for the velocity based on the random walk framework, specifically on the work by Plank and Sleeman [62]. The new model considers the migration of the tip endothelial cells as an stochastic process and defines it as a biased circular random walk. The biasing direction of the random walk represents chemotaxis, whereas the directional randomness is understood as haptotaxis, which acts at a smaller spatial scale.

In the following, we summarize the new model, detailing the definition of the velocity of the tip endothelial cells. First, we describe the continuous equations for the tumor angiogenic factor and the quiescent and stalk endothelial cells. Afterwards, we explain the discrete agents, both for the hypoxic cells and for the tip endothelial cells. At this point, we introduce the biased circular random walk for the tip cells. Then, we proceed describing how the discrete agents at the cellular level are coupled with the macro-scale, continuous equations.

2.1 The continuous problem

The model considers two continuous variables defined in the spatial domain $\Omega \subset \mathbb{R}^d$, where $d = 2, 3$. The first one, f, represents a balance of tumor angiogenic factors released by hypoxic cells that promote the activation of tip endothelial cells and the proliferation of the stalk cells. The second continuous variable, c, is a phase field defining the location of the capillaries in the extracellular matrix. The equation that governs the dynamics of c favors two homogeneous states ($c = 1$ and $c = -1$) that can co-exist stably. The region where $c \geq 0$ represents the capillaries, while $c < 0$ defines the area of the extracellular matrix without capillaries.

The dynamics of the tumor angiogenic factor concentration is governed by the following reaction-diffusion equation

$$\frac{\partial f}{\partial t} = \nabla \cdot (D \nabla f) - B_u f c \mathcal{H}(c) \qquad (1)$$

where D is the diffusion constant, B_u is the uptake rate constant, and $\mathcal{H}(\cdot)$ is the Heaviside function. The first term on the right-hand side of the equation models the diffusion of the tumor angiogenic factor from the hypoxic cells to the remaining part of the extracellular matrix. The second term accounts for the consumption of the factor by the endothelial cells.

The dynamics of the quiescent and stalk endothelial cells is described by the phase-field equation

$$\frac{\partial c}{\partial t} = \nabla \cdot \left(M \nabla \left(\mu_c - \lambda^2 \Delta c \right) \right) + \mathcal{B}_p(f) c \mathcal{H}(c) \qquad (2)$$

where M is the constant mobility, $\mu_c(c) = -c + c^3$ is the chemical potential, and λ is a positive constant proportional to the width of the capillary wall. $\mathcal{B}_p(\cdot)$ is the proliferative rate function, given by

$$\mathcal{B}_p(f) = \begin{cases} B_p f & \text{if } f < f_p \\ B_p f_p & \text{if } f \geq f_p \end{cases}, \qquad (3)$$

Journal: 466 MS: 0958 ☐TYPESET ☐DISK ☐LE ☐CP Disp.:2013/12/13 Pages: 16 Layout: Large

where B_p is the proliferative rate constant and f_p is the tumor angiogenic factor condition for highest proliferation.

The dynamics of Eq. (2) may be understood in the context of phase-field methods. The chemical potential μ_c is the derivative of a double-well potential that energetically favors two homogeneous states separated by a smooth interface. The separation force can be interpreted from a biological standpoint as the driving force that maintains endothelial cells together exerted by the cells themselves. In addition, the second term on the right-hand side accounts for the proliferation of stalk cells in presence of tumor angiogenic factor.

Remarks:

1. In Eq. (2) the value of λ defines the length scale of the problem. As $\lambda \to 0$ the model tends to a sharp interface model [47]. The lower this value, the more accurate is the description of the capillary walls, at the expense of a higher computational cost.
2. The proliferative rate is defined as a piecewise linear function with a plateau that imposes a maximum threshold for proliferation. Hence, this function accounts for the saturation of the tumor angiogenic factor receptors of the surface of the endothelial cells.

2.2 The discrete agents

The model accounts for two types of discrete agents, which represent, respectively, hypoxic and tip endothelial cells. These cells are supposed to be spherical with radii R_{HYC} and R_{TEC}, respectively.

2.2.1 Hypoxic cells

A hypoxic cell is assumed to be a static agent centered at a fixed point that we call generically $\mathbf{x}_{\text{HYC}}$. The agents associated to hypoxic cells have two states: active and inactive. Initially, all the hypoxic cells are distributed in the hypoxic regions of the tissue and are active. While they are active, they produce a fixed amount of angiogenic factor f_{HYC}. Whenever a hypoxic cell becomes normoxic, its associated agent becomes inactive. The model assumes that this situation happens when a capillary is closer than a certain distance, δ_{nox}, which represents the oxygen characteristic diffusion length. An inactive agent does not produce angiogenic factor.

2.2.2 Tip endothelial cells

These agents may be created at any point of the domain or removed according to several criteria. A new agent is created at a point, provided that the following conditions are met: (1) the point is inside a capillary ($c \geq c_{act}$); (2) the tumor angiogenic factor concentration is high enough to stimulate the differentiation of an endothelial cell ($f \geq f_{act}$); (3) the chemotactic signal is strong ($G = \|\nabla f\| \geq G_{act}$); and (4) there is no other tip endothelial cell nearby releasing dll-4 to prevent its differentiation. The characteristic diffusion length of the dll-4 is denoted here by δ_4. If at some point a tip endothelial cell fails to meet these conditions, its associated agent is removed, assuming that the cell changed its phenotype to a non-migratory one.

In contrast to hypoxic cells, tip endothelial cells are mobile. We define the movement of a tip endothelial cell as a biased circular random walk. Let us discretize the time interval of interest, namely $(0, T)$, into N sub-intervals $I_n = (t_{n-1}, t_n)$; $n = 1, \ldots, N$, where $0 = t_0 < t_1 < \cdots < t_N = T$. We call $\Delta t_n = t_n - t_{n-1}$. Given a tip endothelial cell defined by its center, $\mathbf{x}^n_{\text{TEC}} = \left(x^n_{\text{TEC}}, y^n_{\text{TEC}}, z^n_{\text{TEC}}\right)$, at time t_n, we define its trajectory by the set of equations

$$\left.\begin{aligned} x^n_{\text{TEC}} &= x^{n-1}_{\text{TEC}} + \rho\cos(\theta_n)\sin(\varphi_n)\Delta t_n \\ y^n_{\text{TEC}} &= y^{n-1}_{\text{TEC}} + \rho\sin(\theta_n)\sin(\varphi_n)\Delta t_n \\ z^n_{\text{TEC}} &= z^{n-1}_{\text{TEC}} + \rho\cos(\varphi_n)\Delta t_n \end{aligned}\right\}, \tag{4}$$

where ρ, the velocity magnitude, is a deterministic function of the model parameters and the magnitude of the gradient of tumor angiogenic factor concentration. θ_n and φ_n are realizations of the discrete stochastic variables Θ_n and Φ_n which denote, respectively, the azimuthal and the polar (zenith) angles of the spherical system of coordinates. We will assume that Θ_n and Φ_n are independent for all $n > 0$. The range of Θ_n, namely R_{Θ_n}, is defined as

$$R_{\Theta_n} = \{\theta_{n-1} + \delta, \theta_{n-1}, \theta_{n-1} - \delta\} \tag{5}$$

while the range of Φ_n is

$$R_{\Phi_n} = \{\varphi_{n-1} + \delta, \varphi_{n-1}, \varphi_{n-1} - \delta\}\,. \tag{6}$$

Equations (5)–(6) can be straightforwardly applied to the case $n > 1$. When $n = 1$, θ_0 and φ_0 should be understood as deterministic values given by the gradient of the angiogenic factor at the initial time. We denote the azimuthal component of the gradient by θ^{ch}_0 and the polar component by φ^{ch}_0, where the superscript indicates that this is the direction of chemotactic migration. Note that $\{\Theta_n\}_{n>0}$ and $\{\Phi_n\}_{n>0}$ define two Markov chains, as follows from Eqs. (5)–(6), and the independence of Θ_n and Φ_n for all $n > 0$. Eqs. (5)–(6) show that, from one time step to the next and for each angular direction, the tip endothelial cell may turn clockwise or anticlockwise an angle δ or remain advancing in the same direction. The probabilities of these events are given by the probability functions of Θ_n and Φ_n defined as

$$P\left[\Theta_n = \theta_{n-1} + \delta\right] = \hat{\tau}^{+}_{\theta^{\text{ch}}_n}\Delta t_n \tag{7}$$

$$P\left[\Theta_n = \theta_{n-1} - \delta\right] = \hat{\tau}^{-}_{\theta^{\text{ch}}_n}\Delta t_n \tag{8}$$

Journal: 466 MS: 0958 TYPESET DISK LE CP Disp.:2013/12/13 Pages: 16 Layout: Large

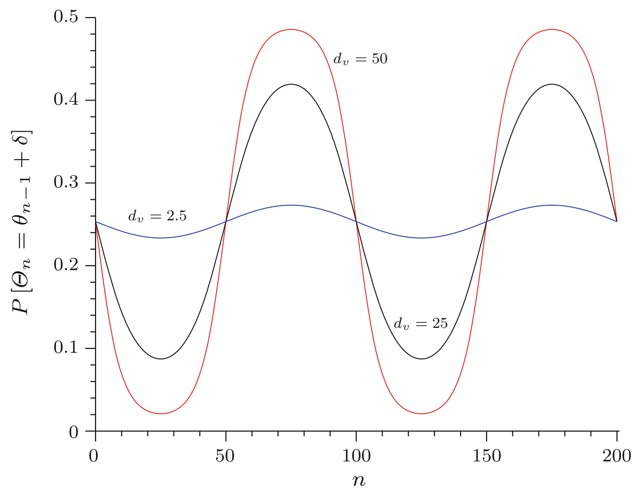

Fig. 1 Probability function of turning anticlockwise through an angle $\delta = \frac{\pi}{50}$ for 200 time steps. We plot three probability functions, each for a different value of the turning rate d_v. The rotational diffusivity is $D_r = 1$, the biased direction is $\theta_0 = 0$, and the time step size is $\Delta t_n = 0.001$

$$P\left[\Theta_n = \theta_{n-1}\right] = \left(1 - \hat{\tau}^{+}_{\theta^{ch}_n} - \hat{\tau}^{-}_{\theta^{ch}_n}\right) \Delta t_n \tag{9}$$

$$P\left[\Phi_n = \varphi_{n-1} + \delta\right] = \hat{\tau}^{+}_{\varphi^{ch}_n} \Delta t_n \tag{10}$$

$$P\left[\Phi_n = \varphi_{n-1} - \delta\right] = \hat{\tau}^{-}_{\varphi^{ch}_n} \Delta t_n \tag{11}$$

$$P\left[\Phi_n = \varphi_{n-1}\right] = \left(1 - \hat{\tau}^{+}_{\varphi^{ch}_n} - \hat{\tau}^{-}_{\varphi^{ch}_n}\right) \Delta t_n \tag{12}$$

where $\hat{\tau}^{+}_{\theta^{ch}_n}$, $\hat{\tau}^{-}_{\theta^{ch}_n}$, $\hat{\tau}^{+}_{\varphi^{ch}_n}$, and $\hat{\tau}^{-}_{\varphi^{ch}_n}$ are the so-called transition rates and θ^{ch}_n and φ^{ch}_n are the azimuthal and polar directions given by the positive gradient of the tumor angiogenic factor at time t_n. The transition rates are given by

$$\hat{\tau}^{\pm}_{\theta^{ch}_n} = 2\nu \frac{\tau_{\theta^{ch}_n}\left(\left(n \pm \frac{1}{2}\right)\delta\right)}{\tau_{\theta^{ch}_n}\left(\left(n + \frac{1}{2}\right)\delta\right) + \tau_{\theta^{ch}_n}\left(\left(n - \frac{1}{2}\right)\delta\right)} \tag{13}$$

$$\hat{\tau}^{\pm}_{\varphi^{ch}_n} = 2\nu \frac{\tau_{\varphi^{ch}_n}\left(\left(n \pm \frac{1}{2}\right)\delta\right)}{\tau_{\varphi^{ch}_n}\left(\left(n + \frac{1}{2}\right)\delta\right) + \tau_{\varphi^{ch}_n}\left(\left(n - \frac{1}{2}\right)\delta\right)} \tag{14}$$

where $\nu = \frac{D_r}{\delta^2}$ and D_r is the so-called rotational diffusivity. The derivation of the transition rates can be found at [60]. The transition probabilities $\tau_{\theta^{ch}_n}$ and $\tau_{\varphi^{ch}_n}$ used in Eqs. (13)–(14) are von Mises probability density functions given by

$$\tau_{\theta^{ch}_n}(\alpha) = \frac{1}{2\pi I_0(\frac{d_v}{D_r})} \exp\left(\frac{d_v}{D_r}\cos(\alpha - \theta^{ch}_n)\right) \tag{15}$$

$$\tau_{\varphi^{ch}_n}(\alpha) = \frac{1}{2\pi I_0(\frac{d_v}{D_r})} \exp\left(\frac{d_v}{D_r}\cos(\alpha - \varphi^{ch}_n)\right) \tag{16}$$

where $I_0(\cdot)$ is the modified Bessel function of the first kind and zeroth order and d_v is the turning coefficient. Figure 1 shows the evolution of the probability function of turning clockwise for 200 time steps and for various values of the turning coefficient.

Following [72], the velocity magnitude of the tip endothelial cell is a function of the norm of the gradient of the tumor angiogenic factor evaluated at the center of the tip endothelial cell, such that

$$\rho = \chi \left\|\nabla f\left(\mathbf{x}_{\text{TEC}}\right)\right\| \mathcal{L}\left(\left\|\nabla f\left(\mathbf{x}_{\text{TEC}}\right)\right\|\right) \tag{17}$$

where χ is a chemotactic constant, the operator $\|\cdot\|$ denotes the Euclidean norm of a vector, and $\mathcal{L}$ is a limiting function defined as

$$\mathcal{L}\left(\|\nabla f\|\right) = 1 + \left(\frac{G_M}{\|\nabla f\|} - 1\right) \mathcal{H}\left(\|\nabla f\| - G_M\right) \tag{18}$$

where G_M is a constant.

2.3 The continuum/discrete coupling

Both the discrete hypoxic cells and tip endothelial cells must be coupled with the continuous equations of the model. First, as said above, hypoxic cells are responsible for the introduction of the tumor angiogenic factor in the system. Hence, these discrete components are coupled with Eq. (1). In the regions occupied by active hypoxic cells the value of the tumor angiogenic factor is constant and equal to f_{HYC}. Second, as discrete tip endothelial cells move, they produce, by proliferation, an excess in the concentration of endothelial cells. Consequently, they are coupled with Eq. (2). The ratio of the material produced in the tip cell to the volume swept as the cell migrates, gives us the value of the order parameter inside the tip endothelial cell. Thus, in the region of the domain occupied by a tip endothelial cell, the order parameter is given by

$$c_{\text{TEC}} = \frac{4\mathcal{B}_p\left(f\left(\mathbf{x}_{\text{TEC}}\right)\right) R_{\text{TEC}}}{3\rho}. \tag{19}$$

2.4 Parameters

As the equations of the mathematical model are written in dimensionless form, we detail the value of all the corresponding dimensionless parameters. However, many of them were matched to or obtained from experiments *in vivo* (see [72] and the references therein). The physical values of these parameters may be retrieved using the length and time scales $L_0 = 1.25\,\mu\text{m}$ and $T_0 = 1560\,\text{s}$.

In Table 1 we show the dimensionless parameters of the continuous Eqs. (1) and (2) in the same order as in the text. The remaining parameters come from the discrete agent description. The radii of the discrete agents, namely R_{HYC} and R_{TEC} are assumed to be equal. Travasso et al. [72], in agreement with [30], fixed the radius of the tip endothelial

Journal: 466 MS: 0958 ☐ TYPESET ☐ DISK ☐ LE ☐ CP Disp.:2013/12/13 Pages: 16 Layout: Large

Table 1 Dimensionless parameters of the continuous Eqs. (1) and (2)

Parameter	Value
Diffusion constant	$D = 100$
Uptake rate constant	$B_u = 6.25$
Constant mobility	$M = 1$
Interface width	$\lambda = 1$
Proliferative rate	$B_p = 1.401$
TAF condition for highest proliferation	$f_p = 0.3$

Table 2 Parameters related to the movement of the tip endothelial cells

Parameter	Value
Chemotactic constant	$\chi = 242.67$
TAF gradient for highest velocity	$G_M = 0.03$
Rotational diffusivity	$D_r = 0.05$
Turning coefficient	$d_v = 25$
Turning angle	$\delta = \frac{\pi}{50}$

cells in 5 µm, which is 4 in the dimensionless formulation of the model. The oxygen diffusion length, δ_{nox}, is 25 µm (20 in dimensionless quantities) as in [38]. The production of tumor angiogenic factor per time step is $f_{\text{HYC}} = 1$. The parameters that determine the activation or deactivation of tip endothelial cells are:

1. Order parameter condition for activation or deactivation $c_{act} = 0.9$.
2. Tumor angiogenic factor condition for activation or deactivation $f_{act} = 0.055$.
3. Tumor angiogenic factor gradient condition for activation or deactivation $G_{act} = 0.01$.
4. Dll-4 diffusion length $\delta_4 = 16$. The value of this parameter *in vivo* is 20 µm.

Finally, in Table 2 we show the dimensionless parameters related to the movement of tip endothelial cells. The value of the rotational diffusivity and the turning coefficient were obtained through a parametric study of the model. The value of the turning angle δ was maintained equal to that proposed in [62].

3 Numerical method

In this section we present a numerical method to solve the mathematical model. As in the model, we naturally divide the algorithm in three blocks: the method for the discrete agents, the method for coupling the discrete and the continuous variables, and the algorithm for solving the continuous equations. In the method for the discrete agents, we first evaluate the discrete rules that determine the activation and deactivation of the agents. This process is simple, so we omit the details of the related algorithms. Therefore, we start this section explaining the method to compute the displacement of the tip endothelial cells following the biased circular random walk. Then, we outline how we solve the coupling between the discrete components and the continuous equations. We close the section explaining the method for solving the continuous equations, which is based on isogeometric analysis [18,43] for the spatial discretization and on the generalized-α method [16,44] for the time discretization.

3.1 The tip endothelial cell motion

After activation/deactivation of the discrete agents in time step t_n, we move each active tip endothelial cell according to Eq. (4). The velocity magnitude ρ is a deterministic function given by Eq. (17) which we evaluate at the center of the tip endothelial cells. The angles that determine the direction, on the contrary, are given by the realizations θ_n and φ_n of the random variables Θ_n and Φ_n, respectively.

We follow the technique used in [62,69] to obtain the value of the realizations. For the direction Θ we generate a random number r with uniform distribution over the interval [0,1] and divide the unit interval in three sub-intervals. If the random number falls into the first sub-interval, $[0, \hat{\tau}_n^+ \Delta t_n)$, then $\theta_n = \theta_{n-1} + \delta$ and the tip endothelial cell turns clockwise through an angle δ; if it falls into the second sub-interval, $[\hat{\tau}_n^+ \Delta t_n, 2\nu \Delta t_n)$, then $\theta_n = \theta_{n-1} - \delta$ and the cell turns anti-clockwise through an angle δ; and if the random number falls into the last sub-interval, $(2\nu \Delta t_n, 1]$, then $\theta_n = \theta_{n-1}$ and the tip endothelial cell continues in its current direction. The realization φ_n is obtained analogously.

Remark Note that equations (7)–(12) impose an upper bound on the time step Δt_n, because all probabilities should remain below one. We think of this restriction as an stability condition for the time-stepping scheme.

3.2 The coupling methodology

We start by giving some definitions for the domains of the discrete agents, following the ideas of the mathematical framework of this model developed in [73]. Recalling that for any time step, each hypoxic cell is characterized by its center and its constant radius, R_{HYC}, we can define Ω^i_{HYC} as the domain occupied by the i-th hypoxic cell, which in three dimensions is a sphere centered at $\mathbf{x}^i_{\text{HYC}}$. Furthermore, we can define the domain of all the active hypoxic cells for a given time step, say t_n, as

$$\Omega_{\text{HYC}}(t_n) = \bigcup_{k \in A_{\text{HYC}}(t_n)} \Omega^k_{\text{HYC}} \tag{20}$$

Journal: 466 MS: 0958 ☐ TYPESET ☐ DISK ☐ LE ☐ CP Disp.:2013/12/13 Pages: 16 Layout: Large

where $A_{\mathrm{HYC}}(t_n)$ is the set of indices of the active hypoxic cells at time t_n.

Similarly, for the same time step we define the domain $\Omega^j_{\mathrm{TEC}}(t_n)$ as the spherical domain occupied by the j-th tip endothelial cell, with radius R_{TEC} and center $\mathbf{x}^j_{\mathrm{TEC}}$. Notice the time dependency of the domain of each tip cell due to its movement, opposed to the hypoxic-cell domains which are time-independent and only the set of indices depends on time, indicating which agents are active. The domain of tip endothelial cells is given by

$$\Omega_{\mathrm{TEC}}(t_n) = \bigcup_{l \in A_{\mathrm{TEC}}(t_n)} \Omega^l_{\mathrm{TEC}}(t_n) \tag{21}$$

where $A_{\mathrm{TEC}}(t_n)$ is the set of indices of tip endothelial cells at time t_n. All of the above-defined domains are subsets of Ω.

These definitions facilitate the coupling between the discrete components and the continuum variables. Therefore, we can now overwrite the value of the tumor angiogenic factor, $f(t_{n-1})$, and the value of the order parameter, $c(t_{n-1})$, in the subdomains $\Omega_{\mathrm{HYC}}(t_n)$ and $\Omega_{\mathrm{TEC}}(t_n)$, with f_{HYC} and c_{TEC}, respectively. Consequently, we would introduce discontinuities in the fields f and c. However, we try to avoid the artificial inclusion of sharp transitions in the continuous variables, for it goes against the philosophy of the phase-field equation. For this purpose we define template functions for f_{HYC} and c_{TEC} that are multidimensional generalizations of the analytical solution to the one-dimensional Cahn–Hilliard equation, a simplified version of Eq. (2). The template functions are continuous and introduce smooth transitions between the fields and the imposed values inside the subdomains of the discrete agents. As shown below, the discrete counterparts of the continuous variables f and c live in the finite dimensional space $\mathcal{V}^h$. For this reason, the template functions must be projected onto the same finite dimensional space $\mathcal{V}^h$ before overwriting the discretized fields.

3.3 The continuous equations

We begin by considering a weak form of Eqs. (1) and (2). Let $\mathcal{V}$ denote the trial solution and the weighting function spaces, which are assumed to be the same. At this point we assume free-flux boundary conditions. Equations (1) and (2) may be recast in variational form by multiplying them with smooth functions, integrating over the domain, and applying integration by parts repeatedly. The problem may be stated as follows: find $f, c \in \mathcal{V}$ such that $\forall w, q \in \mathcal{V}$:

$$\int_\Omega w \frac{\partial f}{\partial t} d\Omega + \int_\Omega \nabla w D \nabla f d\Omega + \int_\Omega w B_u f c \mathcal{H}(c)\, d\Omega$$

$$+ \int_\Omega q \frac{\partial c}{\partial t} d\Omega + \int_\Omega \nabla q M \nabla \mu_c \, d\Omega + \int_\Omega \Delta q M \lambda^2 \Delta c \, d\Omega$$

$$- \int_\Omega q \mathcal{B}_p(f)\, c \mathcal{H}(c)\, d\Omega = 0 \tag{22}$$

The space $\mathcal{V}$ is a subset of $\mathcal{H}^2$, the Sobolev space of square integrable functions with square integrable first and second derivatives. To perform the spatial discretization of the previous weak formulation we make use of the Galerkin method. Let us define the discrete space $\mathcal{V}^h$, which is a subset of $\mathcal{V}$. We approximate (22) by the following variational problem over the finite dimensional space: find $f^h, c^h \in \mathcal{V}^h \subset \mathcal{V}$ such that $\forall w^h, q^h \in \mathcal{V}^h \subset \mathcal{V}$:

$$\int_\Omega w^h \frac{\partial f^h}{\partial t} d\Omega + \int_\Omega \nabla w^h D \nabla f^h d\Omega$$

$$+ \int_\Omega w^h B_u f^h c^h \mathcal{H}\left(c^h\right) d\Omega + \int_\Omega q^h \frac{\partial c^h}{\partial t} d\Omega$$

$$+ \int_\Omega \nabla q^h M \nabla \mu(c^h) d\Omega + \int_\Omega \Delta q^h M \lambda^2 \Delta c^h d\Omega$$

$$- \int_\Omega q^h \mathcal{B}_p\left(f^h\right) c^h \mathcal{H}\left(c^h\right) d\Omega = 0 \tag{23}$$

Here f^h is defined as

$$f^h(\mathbf{x}, t) = \sum_{A=1}^{n_b} f_A(t)\, N_A(\mathbf{x}) \tag{24}$$

where n_b is the dimension of the discrete space $\mathcal{V}^h$ and N_A are the basis functions. The key feature of isogeometric analysis [8,18–20,43], the computational method employed in this work, is that the typical finite-element piecewise-polynomial basis functions are replaced with more general functions frequently used in computational geometry. The coefficients f_A in Eq. (24) are the so-called control variables. The rest of the variables of Eq. (23), namely c^h, w^h, and q^h, are defined analogously to f^h. Since we will use a conforming discretization, the relation $\mathcal{V}^h \subset \mathcal{V}$ holds and the discrete functions are required to be in $\mathcal{H}^2$. This condition is satisfied by the globally $\mathcal{C}^1$-continuous basis functions that we consider in this paper, by means of isogeometric analysis. In this paper we utilize Non-Uniform Rational B-Splines (NURBS) [43] as basis functions, which reduce to B-Splines, in a three-dimensional, cube geometry. For more details about the resolution of higher-order partial differential equations using isogeometric analysis, the reader is referred to [32,35–37], and for alternative approaches outside the classical continuous finite element method, the reader is referred to [6,21,24,63,75].

We integrate in time using the generalized-α method [16,44]. The generalized-α method is a second-order accurate, unconditionally A-stable method with controllable high-frequency dissipation that can be easily implemented within an adaptive time step framework. All these features make it a good choice for highly nonlinear problems [9,10,33] such

Journal: 466 MS: 0958 ☐ TYPESET ☐ DISK ☐ LE ☐ CP Disp.:2013/12/13 Pages: 16 Layout: Large

as that addressed in this paper (for time integrators specifically designed for phase-field models, the reader is referred to [34,53]). In addition, we use a time-step size selection algorithm that considerably reduces the computational time. This algorithm was first proposed in [49] for reaction-diffusion equations and was then utilized for other mathematical models, such as in [32]. After space and time discretization, we obtain a non-linear system which is solved using a predictor multi-corrector algorithm based on the Newton-Raphson method.

4 Results and discussion

We begin this section with an analysis of the tumor angiogenesis model. The analysis is performed through two-dimensional simulations, as the visualization of the patterns created during angiogenesis is easier in this simplified setting. We show in Fig. 2 various snapshots that capture the time evolution of the vascular network. In this simulation we analyze the directionality of the tip endothelial cells, from the initiation of angiogenesis until the complete oxygenation of the tissue. Then, we present the final patterns of four two-dimensional simulations in Figs. 3 and 4. One of the two parameters that determine the biased circular random walk, namely the rotational diffusivity (D_r) and the turning coefficient (d_v), is changed for each pair of simulations. This enables us to study how the frequency and the amplitude of the turnings influence the development of the network. We finalize this section presenting four three-dimensional simulations of the tumor angiogenesis model. The results of the simulations are discussed based on Figs. 5, 6, 7 and videos Online Resources 1–4. In addition, we study through Fig. 8 the effect of haptotaxis in the model presented in Sect. 2. To carry out this study, we compare the previous three-dimensional simulations with the same simulations for a model that only considers chemotaxis.

4.1 Analysis of the model

The five two-dimensional simulations that we present are performed on the square domain $\overline{\Omega} = [0, 300]^2$. This domain represents a tissue of 375 $\times$ 375 μm, although the periodic condition imposed in the horizontal direction, allows the vasculature to spread further than in a tissue of the mentioned size. We have used a regular mesh defined by 128^2 knot spans and quadratic basis functions with $\mathcal{C}^1$-continuity across element boundaries (see [18,43] to understand the basic terminology of isogeometric analysis). In order to facilitate the comparison among the two-dimensional simulations, all the initial conditions are the same: a blood vessel at the bottom of the domain and 200 hypoxic cells randomly scattered on the extracellular matrix according to a uniform distribution. The

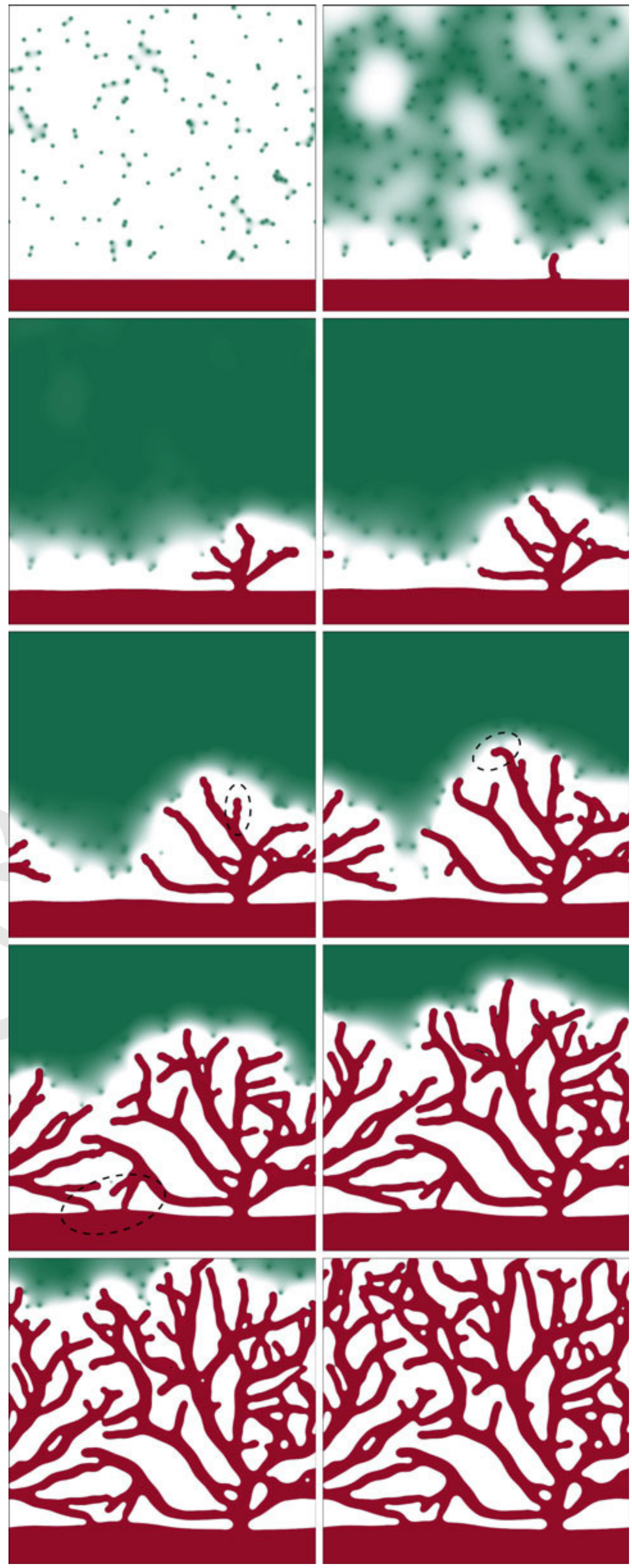

Fig. 2 Formation of a vascular network driven by tumor induced angiogenesis. 200 hypoxic cells produce tumor angiogenic factor (*green*) that promotes the initiation and growth of new sprouts (*red*). The simulation is performed on the domain $\overline{\Omega} = [0, 300]^2$ using the parameters presented in Sect. 2.4

Journal: **466** MS: **0958** ☐ TYPESET ☐ DISK ☐ LE ☐ CP Disp.:**2013/12/13** Pages: **16** Layout: **Large**

Fig. 3 Comparison of the final patterns of two simulations for different values of the rotational diffusivity: 1000 % (*left*) and 10 % (*right*) of D_r. The remaining parameters and conditions of the simulations are the same as those in Fig. 2. Tip endothelial cells constantly change their direction for high values of the rotational diffusivity and do not change it for low values

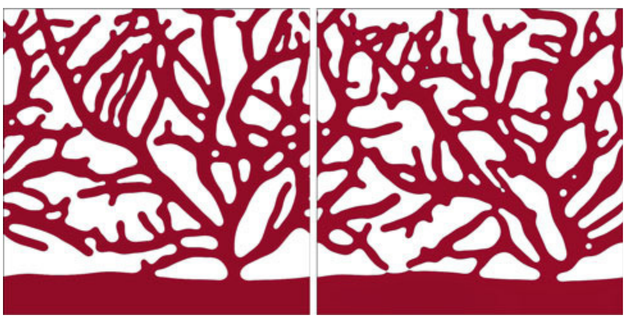

Fig. 4 Comparison of the final patterns of two simulations for different values of the turning coefficient: 200 % (*left*) and 10 % (*right*) of d_v. The remaining parameters and conditions of the simulations are the same as those in Fig. 2. The higher the values of d_v the better tip endothelial cells reorient towards hypoxic cells

radius of the initial vessel is set to 37.5 µm. The first snapshot of Fig. 2 shows these initial conditions, where the red color represents the capillary and the green color represents the tumor angiogenic factor. This color code is maintained for the remaining figures and videos.

Figure 2 shows the initiation and evolution of a new vascular network promoted by an avascular tumor, represented here by its hypoxic region. The simulation uses the parameters of the model presented in Sect. 2.4. At the beginning of the simulation, the 200 hypoxic cells start to release tumor angiogenic factor, which diffuses throughout the domain. The angiogenesis process is initiated when the factor reaches the initial vessel at the bottom of the domain, with enough quantity to activate a tip endothelial cell. Thus, in the second snapshot of Fig. 2 we observe that one tip endothelial cell has become active and has started its migration. At this moment, there is only one of these cells because, the cell itself prevents the differentiation of the surrounding cells into the tip endothelial cell phenotype. The other cells stimulated by the tumor angiogenic factor, instead, attain a proliferative phenotype, generating the capillary behind the tip endothelial cell. However, as the leading cell moves away, new tip endothelial cells get activated, for the delta-like ligand 4 released by the first tip endothelial cell does not reach them anymore. Hence, more sprouts are created and the vascular network spreads. As the network grows, it consumes tumor angiogenic factor and returns the hypoxic cells into their normoxic condition, as shown in the remaining snapshots.

In this simulation we can study the movement of tip endothelial cells. Although the global migration of the leading cells is governed by the gradient of the tumor angiogenic factor, we observe in the simulation how tip endothelial cells turn and reorient towards this gradient. This phenomenon, introduced by the biased circular random walk in the mathematical model, represents our simple conceptualization of haptotaxis. The variation of gradients of non-soluble molecules bounded to the extracellular matrix hinders the movement towards hypoxic cells. Tip endothelial cells find their chemotaxis-driven migration obstructed by a scarcity of non-soluble molecules, so they eventually alter their direction of migration. Additionally, the turns allow the cells to better detect the changes in their micro-environment, as they explore a broader area when they turn. In Fig. 2, several of these turning events are highlighted. For example, in the fifth snapshot (third row, first column) we distinguish a zigzag movement of various tip endothelial cells. This kind of short-angled, high-frequent turns only affect the direction of the capillary growth and do not create zigzag final patterns, for the undulating morphology is afterwards eliminated by the local remodeling of the phase-field equation. When the direction is maintained for a large time because the gradient of non-soluble molecules of the extracellular matrix favors one direction, tip cells do not reorient and the capillaries deviate from their supposed objective (the hypoxic cells). In these cases, the final pattern of the vasculature is significantly altered, as in the sixth snapshot where the highlighted tip endothelial cell turns left although a hypoxic cell is just above it. The previous set of examples shows, as observed in experiments, the relevant role of haptotaxis in the patterns of the vasculature after an angiogenesis event.

In this mathematical model, anastomosis events can occur for two reasons. The first one, also considered in the model without the biased circular random walk, is the distribution of hypoxic cells. In this case, tip cells grow towards the gradient of angiogenic factor and they mainly anastomose at the location of the hypoxic cells. The second cause of anastomosis is the new physics that we added to the model: haptotactic migration. Anastomosis events occur more frequently in our model because tip endothelial cells alter their direction of migration and come across another endothelial cell. One example is in the highlighted area of the seventh snapshot where two capillaries turn towards the initial vessel producing anastomosis, although the hypoxic cell is in the other direction. We can see there that anastomosis events are not

Journal: 466 MS: 0958 ☐ TYPESET ☐ DISK ☐ LE ☐ CP Disp.:2013/12/13 Pages: 16 Layout: Large

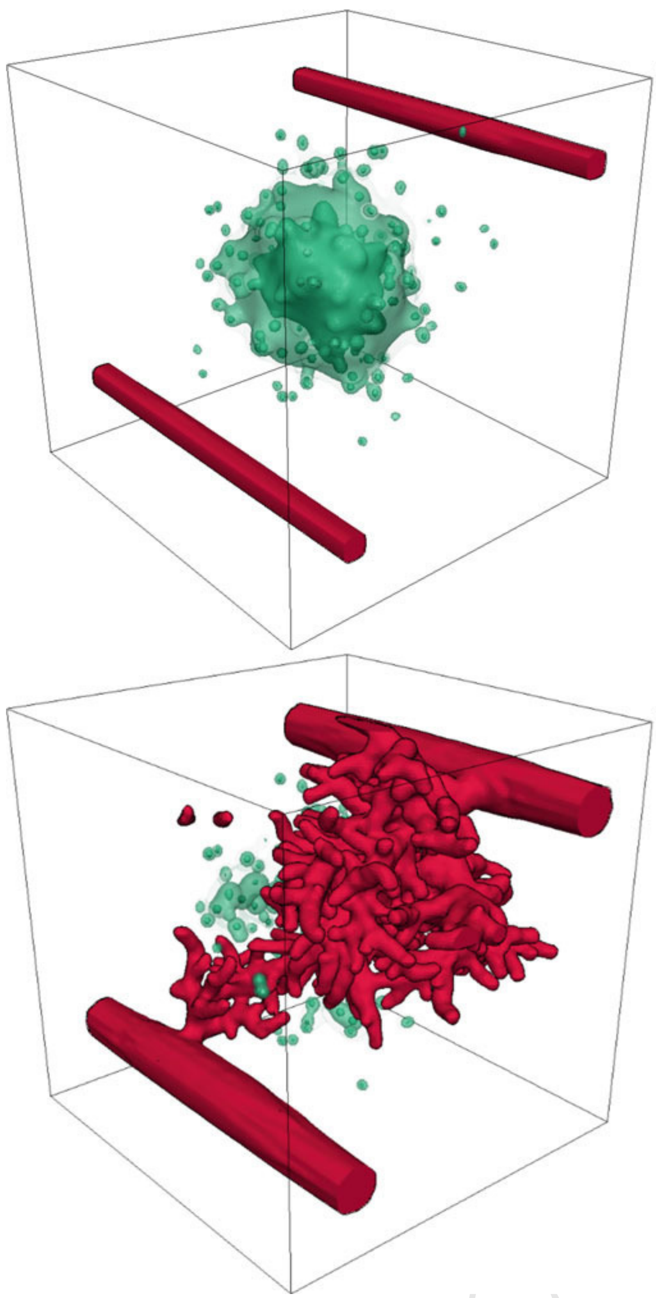

Fig. 5 A new vascular network develops from two parent capillaries. The new sprouts are initiated by the tumor angiogenic factor (*green isosurfaces*) released from hypoxic cells disposed forming a tumor-like structure. The tip endothelial cells that lead the growth of the sprouts migrate by chemotaxis and haptotaxis. At the end of the simulations the vasculature pervades the tumor, leaving no cells under hypoxic conditions. Many anastomosis events create loops in the new vasculature and connect the parent capillaries. The simulation is performed on the domain $\overline{\Omega} = [0, 300]^3$ using the parameters presented in Sect. 2.4

determined by the location of hypoxic cells, but also depend on haptotaxis. In addition, there are more anastomoses than there would be in an identical simulation of the model without the circular biased random walk incorporated (results not shown).

Figures 3 and 4 allow us to further investigate in two dimensions how endothelial cells migrate under different values of two of the parameters that define the biased random walk, namely the rotational diffusivity D_r and the turning coefficient d_v. We maintain the remaining parameters and initial conditions equal to those in the simulation of Fig. 2, for the sake of an easier comparison. Thus, for the two simulations in Fig. 3 we alter the value of the rotational diffusivity. In the simulation on the left-hand side the value of the para-

Journal: **466** MS: **0958** ☐ TYPESET ☐ DISK ☐ LE ☐ CP Disp.:**2013/12/13** Pages: **16** Layout: **Large**

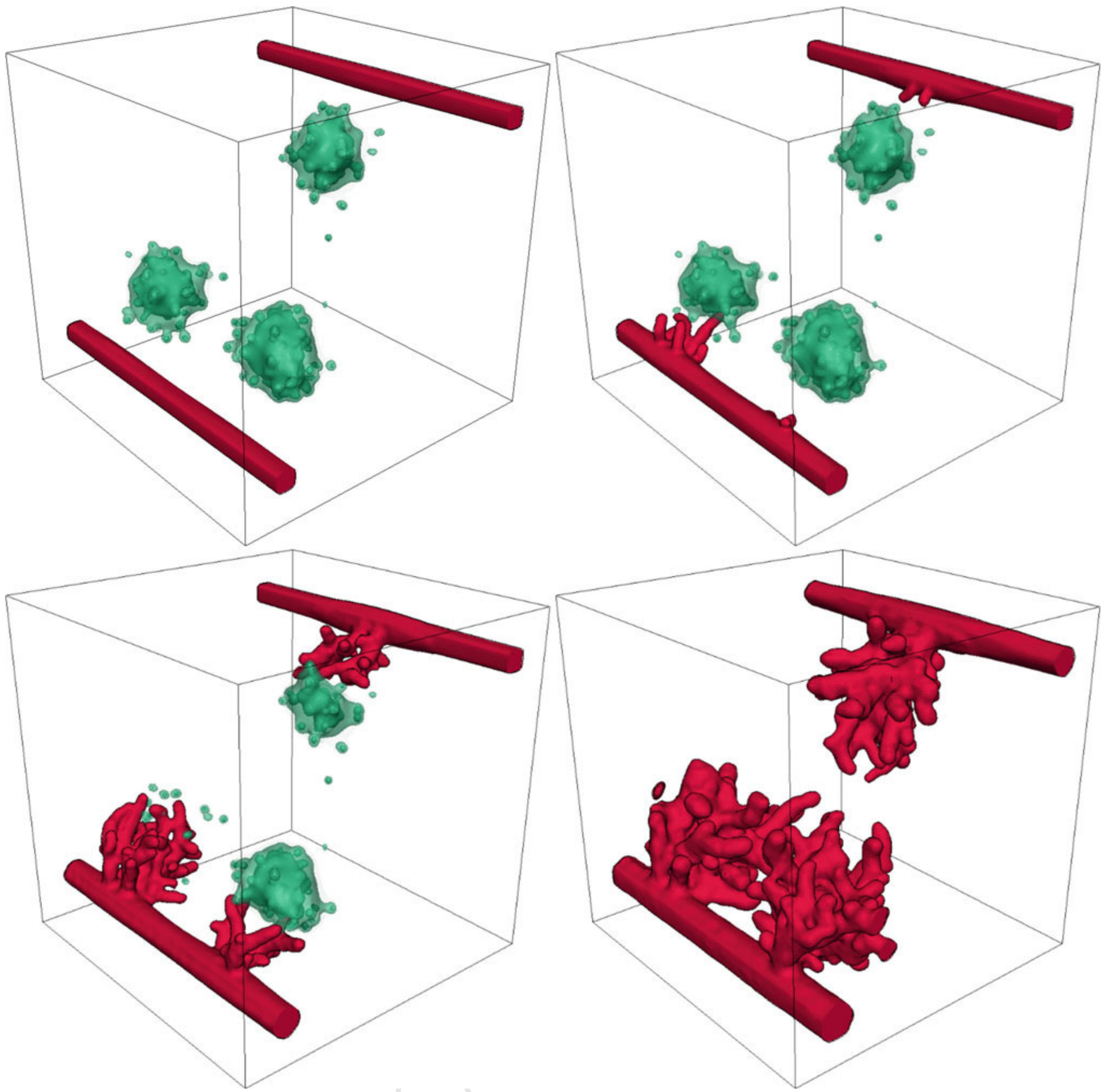

Fig. 6 Evolution of a vascular network promoted by hypoxic cells mimicking a multifocal tumor. Three sets of sprouts grow from the initial capillaries until there are not hypoxic cells. The simulation is performed on the domain $\overline{\Omega} = [0, 300]^3$ using the parameters presented in Sect. 2.4

meter is 1000 % of D_r and in that of the right-hand side, it is 10 % of D_r. The final patterns of both simulations are drastically different. In the first one, since the rotational diffusivity is increased, the frequency at which the turns occur is too high for tip endothelial cells to lead the capillaries towards the hypoxic cells following a smooth curve. This may be interpreted as a vascular network developing within an extracellular matrix with very low concentration of non-soluble molecules or focal adhesion sites. The tip endothelial cells in this situation wander in small regions, trying to find a migration path. In contrast, in the second simulation, the low value of the rotational diffusivity almost impedes the tip endothelial cells to deviate from its original trajectory. In this case, the distribution of the non-soluble chemoattractants or of the focal adhesion sites may be thought of as strongly biased in some preferential directions. The resulting capillaries are highly tortuous in the first simulation and too straight in the second.

Journal: **466** MS: **0958** TYPESET DISK LE CP Disp.:**2013/12/13** Pages: **16** Layout: **Large**

Fig. 7 Formation of two vascular networks with disguising characteristics. The capillaries in the first simulation (the three snapshots in the *upper row*) promoted by 200 hypoxic cells are thinner than those in the second simulation (*bottom row*), which are promoted by 100 hypoxic cells. In addition the first vasculature is composed of a higher number of capillaries

In Fig. 4, in the simulation on the left-hand side, the value of the turning coefficient is 200 % of d_v and in that of the right-hand side, it is 10 % of d_v. When the value of the turning coefficient is high, the ability of tip endothelial cells to reorient towards the preferred direction at each turn is increased, while when it is low, for the same value of the rotational diffusivity, the reorientation is hindered. We observe in the figure that the tip endothelial cells on the left-hand-side simulation tend to go rapidly towards the hypoxic cells, compared to the simulation on the right-hand side. The reason is that the bias of the random walk is increased on the left-hand-side simulation, so the chemotatic direction is highly favored. In addition, the higher the value of the turning coefficient the lower the number of anastomoses that are not promoted by the distribution of the hypoxic cells.

4.2 Three-dimensional simulations

The numerical method developed in Sect. 3 permits us to perform three-dimensional simulations of our tumor angiogenesis model. All the simulations are performed on the computational domain $\overline{\Omega} = [0, 300]^3$, which represents a cube with side length 375 µm. We use quadratic basis functions and a uniform mesh defined by the tensor product of open knot vectors, each composed by 72 knots. The boundary conditions are no-flux conditions in all the directions, except in the direction parallel to the axis of the initial capillaries, where the domain is periodic. Therefore, as in the two-dimensional simulations, we allow the capillaries to spread in the mentioned direction forming more connected patterns.

4.2.1 Angiogenesis triggered by a cluster of hypoxic cells

Here, we analyze two simulations (Figs. 5, 6 and Online Resources 1 and 2), showing four snapshots of the dynamic evolution of the vasculature. The first snapshot of each simulation represents the initial conditions, while the rest are snapshots of relevant situations during the development of the vasculature.

The simulations differ from each other in the initial conditions, while all the parameters are kept constant and equal to those described in Sect. 2.4. For both simulations, we set two initial capillaries, rectilinear and parallel, which traverse the domain from one face of the cube to the opposite, being

Journal: 466 MS: 0958 TYPESET DISK LE CP Disp.:2013/12/13 Pages: 16 Layout: Large

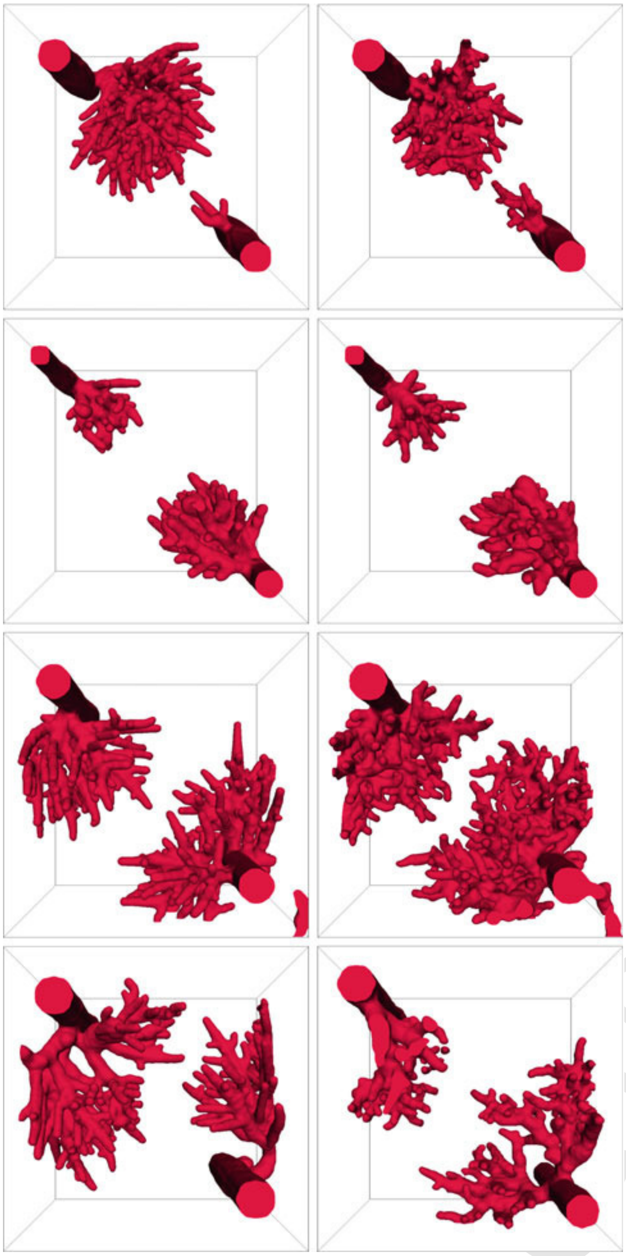

Fig. 8 Influence of haptotaxis in angiogenesis. *Left column* Four simulations (corresponding to Figs. 5, 6, 7), but assuming no haptotactic migration. *Right column* The same four simulations (identical parameters and initial conditions), but including haptotaxis in the model. The patterns of the vasculature differ in tortuosity, number of anastomosis events (connectivity) and length of the capillaries

the axis of the capillaries perpendicular to both faces. This configuration allows angiogenesis to be initiated in both capillaries and increases the number of anastomoses. The initial diameter of the capillaries is constant and equal to 12.5 μm, in accordance with the data from the literature [68]. The difference in the initial conditions comes from the distribution and number of hypoxic cells. In the first simulation (Fig. 5), we set 200 hypoxic cells with locations that follow a normal distribution and mimic a tumor centered in the domain. In the second example (Fig. 6), we set 300 hypoxic cells that aim to represent a three-focus tumor.

In Figs. 5 and 6, we observe the initiation and development of two vascular networks driven by the presence of hypoxic cells disposed in tumor-like structures. In both simulations, the tumor angiogenic factor, represented by green isosurfaces, diffuses from hypoxic cells until it reaches the initial capillaries. At that moment, new capillaries are initiated in the regions where hypoxic cells are closer to the initial capillaries.

In the first simulation (Fig. 5), new sprouts appear first in the upper capillary and they grow forming a network while they consume the tumor angiogenic factor. Meanwhile, the factor reaches the other capillary and several tip endothelial cells become active and start its migration. Both networks continue growing, turning hypoxic cells into normoxic on their way. Towards the end of the simulation, both networks get connected through various anastomoses, allowing the blood to flow between the two main capillaries. The virtual tumor at the center of the domain is now completely pervaded by tortuous capillaries that may trigger the uncontrolled growth of the tumor.

In the second simulation (Fig. 6), the tumor angiogenic factor activates tip endothelial cells in three regions of the initial capillaries in a short time span, as shown in the second snapshot of the simulation. Thus, the three groups of new sprouts grow at a similar rate and almost at the same time. The third snapshot of the simulation shows a plain example of the effect of the biased circular random walk. In the set of sprouts that grow from the upper initial capillary, there are three of them which are led by tip endothelial cells that instead of migrating towards the hypoxic tumor regions grow towards the observer. As shown in Sect. 4.1, in two-dimensional settings this migration driven by haptotaxis usually leads to anastomosis events. However, in three dimensions the probability of a tip endothelial cell coming across a capillary is significantly smaller. As shown in the last snapshot, in this specific case, the three sprouts just stop their growth when there is no more angiogenic factor without anastomosing the two main capillaries.

In all the examples the simulation ends when there is no more tumor angiogenic factor, i.e. no more hypoxic regions are present in the domain. This model does not account neither for the vascular shutdown produced by the high interstitial pressure inside the tumor, nor for the characteristic capillary regression and regrowth (vascular remodeling) after the shutdown events. We think that this is the reason why when both simulations are compared to in vivo tumor images one may observe differences in the patterns (see Fig. 1 in [45] where some tumors present hypoxic regions).

Journal: 466 MS: 0958 TYPESET DISK LE CP Disp.:2013/12/13 Pages: 16 Layout: Large

4.2.2 Angiogenesis triggered by randomly distributed hypoxic cells

In Fig. 7 and Online Resources 3 and 4, we present two simulations (top and bottom of the figure) whereby we can analyze the influence of the number of hypoxic cells when they are randomly distributed. The initial distribution of capillaries is identical to that of the previous examples. On the snapshots of the initial conditions (left-hand-side column of Fig. 7) the position and number of hypoxic cells is revealed by the isosurfaces of the tumor angiogenic factor: 200 for the first simulation (top) and 100 for the second (bottom). As shown on the remaining snapshots, the difference in the number of hypoxic cells promotes the creation of vascular patterns with distinguishing characteristics. There are two main differences, noticeable by simple observation: the thickness and number of capillaries. Both differences are intimately related. For example, in the first simulation, more hypoxic cells initiate more capillaries which consume the tumor angiogenic factor in a high-rate manner. They leave less tumor angiogenic factor per branch for the proliferation of the stalk endothelial cells, and, consequently, the capillaries are thinner. Nevertheless, in the second simulation, as less sprouts appear, each branch has more angiogenic factor and more stalk cells proliferate, enlarging the capillaries. Another difference is in the time of initiation of new branches, being shorter for the first simulation. In the second, the branching is delayed due to a lower number of hypoxic cells, which in turn, leads to a lower concentration of angiogenic factor, and delays the initiation of new sprouts at the beginning. As the network evolves, initiation events occur more and more frequently because the tumor angiogenic factor has enough time to diffuse throughout the extracellular matrix.

4.2.3 Importance of haptotaxis

In Fig. 8 we present four pairs of numerical simulations at an advanced time stage of the network development, each pair corresponding to one of the rows of the figure. In the snapshots on the left-hand side we present the same numerical simulations we described in the previous sections (and in the same order), but considering no haptotactic migration. Each of these simulations has an associated simulation presented on the right-hand side of the figure, which represents exactly the same setting and conditions that its left-hand-side counterpart, but considering haptotaxis in the model.

We omitted the representation of the tumor angiogenic factor, in order to focus on the different vascular morphologies generated by the original model [72] and our model. We observe that the growth patterns are dissimilar in various aspects. The most prominent difference is the tortuosity of the sprouts. Thus, in the simulations of the extended model, tip endothelial cells randomly deviate from the path marked by the gradient of angiogenic factor and create more tortuous capillaries. In contrast, in the simulations on the left-hand side, the tip endothelial cells go directly towards the hypoxic cells resulting in straighter capillaries. The second observable difference is that the number of anastomoses is higher in our model, leading to more connected vasculatures. This leads to a third fundamental difference between the morphology of the networks of both models: the capillaries are shorter in the proposed model because their growth is stopped by anastomosis. Note that these dissimilarities between the models are clearer in the three-dimensional settings than in the two-dimensional ones.

5 Conclusions and future work

Tumor-induced angiogenesis is a complex biological phenomenon and our understanding of it is still limited. However, it is widely accepted that the migration of tip endothelial cells during the growth of new capillaries is driven by three migration mechanisms: chemotaxis, haptotaxis and mechanotaxis. In this paper, we coupled an existing continuum theory with a random walk model, to develop a generalized mathematical model that accounts for chemotaxis and a simple modelization of haptotaxis. We also proposed accurate and efficient algorithms to approximate the solution to the model.

Our model and algorithms provide a framework to perform *in silico* three-dimensional experiments and to study the role of haptotaxis and its interaction with chemotaxis in angiogenesis. Our results indicate that haptotaxis may have a significant impact in the final pattern achieved by capillary networks. The three-dimensional computations presented in this paper also suggest that, for mathematical models to achieve the topological complexity observed in in vivo angiogenesis experiments, two-dimensional simulations may not be enough. We also believe that the accurate modeling of anastomosis, a crucial process in tumor angiogenesis, may require full-scale three-dimensional simulation.

As future work, we believe that a robust and automated quantitative method is needed both for the analysis of mathematical models of angiogenesis and for model validation. We also plan to extend the model to include mechanotaxis and vascular remodeling.

Acknowledgments HG was partially supported by the European Research Council through the FP7 Ideas Starting Grant program (Project #307201) and by *Consellería de Educación e Ordenación Universitaria de la Xunta de Galicia*. IC was partially supported by *Consellería de Educación e Ordenación Universitaria de la Xunta de Galicia* (Grant #CN2011/002). This support is gratefully acknowledged.

References

1. Alarcón T, Byrne HM, Maini PK (2003) A cellular automaton model for tumour growth in inhomogeneous environment. J Theor Biol 225(2):257–274

2. Alarcón T, Byrne HM, Maini PK (2005) A multiple scale model for tumor growth. Multiscale Model Simul 3(2):440–475
3. Alberts B, Johnson A, Lewis J, Raff M, Roberts K, Walter P (2007) Molecular biology of the cell. Garland Science, Oxford
4. Anderson ARA, Chaplain MAJ (1998) Continuous and discrete mathematical models of tumor-induced angiogenesis. Bull Math Biol 60(5):857–899
5. Anderson ARA, Chaplain MAJ (1998) A mathematical model for capillary network formation in the absence of endothelial cell proliferation. Appl Math Lett 11(3):109–114
6. Arroyo M, Ortiz M (2006) Local maximum-entropy approximation schemes: a seamless bridge between finite elements and meshfree methods. Int J Numer Methods Eng 65(13):2167–2202
7. Bauer AL, Jackson TL, Jiang Y (2007) A cell-based model exhibiting branching and anastomosis during tumor-induced angiogenesis. Biophys J 92(9):3105–3121
8. Bazilevs Y, Calo VM, Cottrell JA, Evans JA, Hughes TJR, Lipton S, Scott MA, Sederberg TW (2010) Isogeometric analysis using T-splines. Comput Methods Appl Mech Eng 199(5–8):229–263
9. Bazilevs Y, Calo VM, Zhang Y, Hughes TJR (2006) Isogeometric fluid-structure interaction analysis with applications to arterial blood flow. Comput Mech 38(4–5):310–322
10. Bazilevs Y, Michler C, Calo VM, Hughes TJR (2010) Isogeometric variational multiscale modeling of wall-bounded turbulent flows with weakly enforced boundary conditions on unstretched meshes. Comput Methods Appl Mech Eng 199(13–16):780–790
11. Bentley K, Mariggi G, Gerhardt H, Bates PA (2009) Tipping the balance: robustness of tip cell selection, migration and fusion in angiogenesis. PLoS Comput Biol 5(10):e1000,549
12. Bergers G, Benjamin LE (2003) Angiogenesis: tumorigenesis and the angiogenic switch. Nat Rev Cancer 3(6):401
13. Capasso V, Morale D (2009) Stochastic modelling of tumour-induced angiogenesis. J Math Biol 58(1–2):219–233
14. Chaplain MAJ (2000) Mathematical modelling of angiogenesis. J Neuro-Oncol 50(1–2):37–51
15. Chaplain MAJ, Anderson ARA (1996) Mathematical modelling, simulation and prediction of tumour-induced angiogenesis. Invasion Metastasis 16(4–5):222–234
16. Chung J, Hulbert GM (1993) A time integration algorithm for structural dynamics with improved numerical dissipation: the generalized-α method. J Appl Mech 60:371–375
17. Codling EA, Plank MJ, Benhamou S (2008) Random walk models in biology. J R Soc Interface 5(25):813–834
18. Cottrell JA, Hughes TJR, Bazilevs Y (2009) Isogeometric analysis: toward integration of CAD and FEA. Wiley, Chichester
19. Cottrell JA, Hughes TJR, Reali A (2007) Studies of refinement and continuity in isogeometric structural analysis. Comput Methods Appl Mech Eng 196(41–44):4160–4183
20. Cottrell JA, Reali A, Bazilevs Y, Hughes TJR (2006) Isogeometric analysis of structural vibrations. Comput Methods Appl Mech Eng 195(41–43):5257–5296
21. Cyron CJ, Arroyo M, Ortiz M (2009) Smooth, second order, non-negative meshfree approximants selected by maximum entropy. Int J Numer Methods Eng 79(13):1605–1632
22. Decuzzi P, Causa F, Ferrari M, Netti PA (2006) The effective dispersion of nanovectors within the tumor microvasculature. Ann Biomed Eng 34(4):633–641
23. Dias Soares Quinas Guerra MM, Travasso RDM (2012) Novel approach to vascular network modeling in 3d. In: Bioengineering (ENBENG), 2012 IEEE 2nd Portuguese Meeting in, pp. 1–6
24. Engel G, Garikipati K, Hughes TJR, Larson MG, Mazzei L, Taylor RL (2002) Continuous/discontinuous finite element approximations of fourth-order elliptic problems in structural and continuum mechanics with applications to thin beams and plates, and strain gradient elasticity. Comput Methods Appl Mech Eng 191(34):3669–3750
25. Figg WD, Folkman J (2011) Angiogenesis: an integrative approach from science to medicine. Springer, New York
26. Folkman J (1971) Tumor angiogenesis: therapeutic implications. New Engl J Med 285(21):1182–1186
27. Folkman J, Kalluri R (1984) Tumor angiogenesis. Holland–Frei cancer medicine, 6th edn. BC Decker Inc., Hamilton, pp 161–194
28. Frieboes H, Wu M, Lowengrub J, Decuzzi P, Cristini V (2013) A computational model for predicting nanoparticle accumulation in tumor vasculature. PLoS ONE 8(2):e5687
29. Frieboes HB, Jin F, Chuang YL, Wise SM, Lowengrub JS, Cristini V (2010) Three-dimensional multispecies nonlinear tumor growth-II: tumor invasion and angiogenesis. J Theor Biol 264(4):1254–1278
30. Gebb S, Stevens T (2004) On lung endothelial cell heterogeneity. Microvasc Res 68(1):1–12
31. Gerhardt H, Golding M, Fruttiger M, Ruhrberg C, Lundkvist A, Abramsson A, Jeltsch M, Mitchell C, Alitalo K, Shima D, Betsholtz C (2003) VEGF guides angiogenic sprouting utilizing endothelial tip cell filopodia. J Cell Biol 161(6):1163–1177
32. Gomez H, Calo VM, Bazilevs Y, Hughes TJR (2008) Isogeometric analysis of the Cahn–Hilliard phase-field model. Comput Methods Appl Mech Eng 197(49–50):4333–4352
33. Gomez H, Cueto-Felgueroso L, Juanes R (2013) Three-dimensional simulation of unstable gravity-driven infiltration of water into a porous medium. J Comput Phys 238:217–239
34. Gomez H, Hughes TJR (2011) Provably unconditionally stable, second-order time-accurate, mixed variational methods for phase-field models. J Comput Phys 230:5310–5327
35. Gomez H, Hughes TJR, Nogueira X, Calo VM (2010) Isogeometric analysis of the isothermal Navier–Stokes–Korteweg equations. Comput Methods Appl Mech Eng 199(25–28):1828–1840
36. Gomez H, Nogueira X (2012) An unconditionally energy-stable method for the phase field crystal equation. Comput Methods Appl Mech Eng 249–252:52–61
37. Gomez H, París J (2011) Numerical simulation of asymptotic states of the damped Kuramoto–Sivashinsky equation. Phys Rev E 83:046,702
38. Grote J (1989) Tissue respiration. In: Schmidt R, Thews G (eds) Hum Physiol. Springer, Berlin Heidelberg, pp 598–612
39. Hanahan D, Weinberg RA (2000) The hallmarks of cancer. Cell 100(1):57–70
40. Hanahan D, Weinberg RA (2011) Hallmarks of cancer: the next generation. Cell 144(5):646–674
41. Hellström M, Phng LK, Hofmann JJ, Wallgard E, Coultas L, Lindblom P, Alva J, Nilsson AK, Karlsson L, Gaiano N, Yoon K, Rossant J, Iruela-Arispe ML, Kalén M, Gerhardt H, Betsholtz C (2007) Dll4 signalling through Notch1 regulates formation of tip cells during angiogenesis. Nature 445(7129):776–780
42. Hill N, Häder DP (1997) A biased random walk model for the trajectories of swimming micro-organisms. J Theor Biol 186(4):503–526
43. Hughes TJR, Cottrell JA, Bazilevs Y (2005) Isogeometric analysis: CAD, finite elements, NURBS, exact geometry and mesh refinement. Comput Methods Appl Mech Eng 194(39–41):4135–4195
44. Jansen KE, Whiting CH, Hulbert GM (2000) A generalized-α method for integrating the filtered Navier–Stokes equations with a stabilized finite element method. Comput Methods Appl Mech Eng 190(3–4):305–319
45. Kaanders JH, Bussink J, van der Kogel AJ (2004) Clinical studies of hypoxia modification in radiotherapy. Semin Radiat Oncol 14(3):233–240
46. Knowles M, Selby P (2005) Introduction to the cellular and molecular biology of cancer. Oxford University Press Inc., New York
47. Kobayashi R (1994) A numerical approach to three-dimensional dendritic solidification. Exp Math 3(1):59–81

Journal: 466 MS: 0958 ☐ TYPESET ☐ DISK ☐ LE ☐ CP Disp.:2013/12/13 Pages: 16 Layout: Large

48. Lamalice L, Le Boeuf F, Huot J (2007) Endothelial cell migration during angiogenesis. Circ Res 100(6):782–794
49. Lang J (1995) Two-dimensional fully adaptive solutions of reaction–diffusion equations. Appl Numer Math 18(1–3):223–240
50. Lee TR, Chang YS, Choi JB, Liu WK, Kim YJ (2009) Numerical simulation of a nanoparticle focusing lens in a microfluidic channel by using immersed finite element method. J Nanosci Nanotechnol 9(12):7407–7411
51. Levine HA, Pamuk S, Sleeman BD, Nilsen-Hamilton M (2001) Mathematical modeling of capillary formation and development in tumor angiogenesis: penetration into the stroma. Bull Math Biol 63:801–863
52. Levine HA, Sleeman BD, Nilsen-Hamilton M (2001) Mathematical modeling of the onset of capillary formation initiating angiogenesis. J Math Biol 42(3):195–238
53. Liu J, Gomez H, Evans JA, Hughes TJ, Landis CM (2013) Functional entropy variables: a new methodology for deriving thermodynamically consistent algorithms for complex fluids, with particular reference to the isothermal Navier-Stokes-Korteweg equations. J Comput Phys 248:47–86
54. Lowengrub JS, Frieboes HB, Jin F, Chuang YL, Li X, Macklin P, Wise SM, Cristini V (2010) Nonlinear modelling of cancer: bridging the gap between cells and tumours. Nonlinearity 23(1):R1–R9
55. Macklin P, McDougall S, Anderson ARA, Chaplain MAJ, Cristini V, Lowengrub JS (2009) Multiscale modelling and nonlinear simulation of vascular tumour growth. J Math Biol 58(4–5):765–798
56. Mantzaris NV, Webb S, Othmer HG (2004) Mathematical modeling of tumor-induced angiogenesis. J Math Biol 49(2):111–187
57. McDougall SR, Watson MG, Devlin AH, Mitchell CA, Chaplain MAJ (2012) A hybrid discrete-continuum mathematical model of pattern prediction in the developing retinal vasculature. Bull Math Biol 74(10):2272–2314
58. Milde F, Bergdorf M, Koumoutsakos P (2008) A hybrid model for three-dimensional simulations of sprouting angiogenesis. Biophys J 95(7):3146–3160
59. Orme ME, Chaplain MAJ (1997) Two-dimensional models of tumour angiogenesis and anti-angiogenesis strategies. Math Med Biol 14(3):189–205
60. Othmer HG, Stevens A (1997) Aggregation, blowup, and collapse: the abc's of taxis in reinforced random walks. Siam J Appl Math 57(4):1044–1081
61. Plank MJ, Sleeman BD (2003) A reinforced random walk model of tumour angiogenesis and anti-angiogenic strategies. Math Med Biol 20(2):135–181
62. Plank MJ, Sleeman BD (2004) Lattice and non-lattice models of tumour angiogenesis. Bull Math Biol 66(6):1785–1819
63. Rosolen A, Millán D, Arroyo M (2013) Second-order convex maximum entropy approximants with applications to high-order PDE. Int J Numer Methods Eng 94(2):150–182
64. Scianna M, Bell C, Preziosi L (2013) A review of mathematical models for the formation of vascular networks. J Theor Biol 333:174–209
65. Scianna M, Munaron L, Preziosi L (2011) A multiscale hybrid approach for vasculogenesis and related potential blocking therapies. Prog Biophys Mol Biol 106(2):450–462
66. Scianna M, Preziosi L, Wolf K (2013) A cellular potts model simulating cell migration on and in matrix environments. Math Biosci Eng 10(1):235–261
67. Sciumè G, Shelton S, Gray WG, Miller CT, Hussain F, Ferrari M, Decuzz P, Schrefler BA (2013) A multiphase model for three-dimensional tumor growth. New J Phys 15:015005
68. Shiu YT, Weiss JA, Hoying JB, Iwamoto MN, Joung IS, Quam CT (2005) The role of mechanical stresses in angiogenesis. Crit Rev Biomed Eng 33(5):431–510
69. Sleeman B, Wallis IP (2002) Tumour induced angiogenesis as a reinforced random walk: modelling capillary network formation without endothelial cell proliferation. Math Comput Model 36(3):339–358
70. Stephanou A, McDougall SR, Anderson ARA, Chaplain MAJ (2005) Mathematical modelling of flow in 2D and 3D vascular networks: applications to anti-angiogenic and chemotherapeutic drug strategies. Math Comput Model 41(10):1137–1156
71. Sun S, Wheeler MF, Obeyesekere M, Patrick CW (2005) A deterministic model of growth factor-induced angiogenesis. Bull Math Biol 67(2):313–337
72. Travasso RDM, Poiré EC, Castro M, Rodríguez-Manzanequ JC, Hernández-Machado A (2011) Tumor angiogenesis and vascular patterning: a mathematical model. PLoS One 6(5):e19,989
73. Vilanova G, Colominas I, Gomez H (2013) Capillary networks in tumor angiogenesis: from discrete endothelial cells to phase-field averaged descriptions via isogeometric analysis. Int J Numer Methods Biomed Eng 29(10):1015–1160
74. Weinberg R (1998) One renegade cell: how cancer begins. Basic Books, New York
75. Xia Y, Xu Y, Shu CW (2007) Local discontinuous Galerkin methods for the Cahn–Hilliard type equations. J Comput Phys 227(1):472–491

Journal: 466 MS: 0958 ☐ TYPESET ☐ DISK ☐ LE ☐ CP Disp.:2013/12/13 Pages: 16 Layout: Large